Landscape of the island of stability with self-consistent mean-field potentials

L. A. Malov, G. G. Adamian, and N. V. Antonenko
Joint Institute for Nuclear Research, 141980 Dubna, Russia

H. Lenske
Institut für Theoretische Physik der Justus-Liebig-Universität, D-35392 Gießen, Germany

(Received 10 September 2021; accepted 24 November 2021; published 6 December 2021)

Incorporating effective nucleon mass from the noncovariant energy-density functional, the Schrödinger-equivalent central and spin-orbit mean-field potentials are determined and used in the microscopic-macroscopic method to calculate the ground-state shell corrections in superheavy nuclei with the charge numbers $Z = 112$–126. The island of stability of superheavy nuclei is found to be rather flat and looks like one of coral reef origin due to the interplay between the proton shells at $Z = 114$ and 120, and neutron shells at $N = 174$ and 184, respectively. The shape coexistence in superheavy nuclei depends on spin-orbit potentials and can affect the spectrum of α decay. The one-quasiparticle spectra, isomeric states, and possible α-decay energies are predicted in the nuclei of α-decay chains of $^{295}119$ and $^{295\text{–}297,299}120$.

DOI: 10.1103/PhysRevC.104.064303

I. INTRODUCTION

Experiments on the synthesis of superheavy nuclei (SHN) with charge numbers $Z = 112$–118 [1–11] reveal the existence of an island of stability for the heaviest nuclei. Although the present data do not allow us to fix the center and boarders of this island, they provide some clue for a theory to predict what the island of stability looks like: whether it is a shape resembling a volcanic island of a well-centered distribution of stable SHN, or forms a "coral reef" with stable SHN distributed over an archipelago of binding energy peaks.

The structure of SHN is well described and predicted either with microscopic-macroscopic (MM) approaches [12–14] or with self-consistent many-body methods [15–22]. While the MM approaches rely strongly on the parametrization of single-particle potential and nuclear shape, the self-consistent methods start from energy-density functionals (EDFs). The EDF method is numerically rather involved, especially if deformed nuclei are treated. For exploratory studies of the SHN, the MM method has the clear advantage of allowing rather quick, but reliable estimates of the shell evolution as a function of mass (charge) number. We know that in the region of SHN the MM approaches [12–14] mainly indicate the proton shell closure at $Z = 114$, while the nonrelativistic and relativistic [relativistic mean field (RMF)] self-consistent approaches predict stronger shell effect at $Z = 120$–126. To improve the description of low-lying quasiparticle states, the parameters of the phenomenological single-particle potentials were adjusted in Refs. [23–25] accordingly. After this modification the proton shell closure drifts also in the MM approach from $Z = 114$ to $Z = 120$.

Because of different starting points of MM and self-consistent methods, there is a problem of explaining the difference in their predictions for the SHN properties. This observation points to the connection between the MM and EDF approaches. In Refs. [26,27], the MM and self-consistent methods have been related by incorporating the self-consistently derived central Hartree-Fock-Bogoliubov (HFB) mean-field potentials [28,29] into the MM method. A general scheme has been provided for converting the central mean-field potentials obtained from the nonrelativistic and covariant EDFs into the Schrödinger-equivalent single-particle potentials, appropriate for the MM method. These central potentials are defined under the constraint that we obtain an effective wave equation with a kinetic energy operator containing only a constant mass term in order to comply with the MM method. Thus, the task was to project the density-dependent effective mass contributions from the kinetic operators to the potential, while retaining the essential features of the microscopic self-consistent mean fields. In Refs. [30,31], the mean-field potential was extracted from the EDF based on the Gogny D1S force.

In Refs. [26,27], the spin-orbit single-particle potentials were not obtained from the nonrelativistic EDF but taken phenomenologically. The relativistic EDF provides us with a functional form of spin-orbit potentials that are closely related to the corresponding effective masses. In Ref. [32], we defined the spin-orbit mean-field potentials in terms of the effective masses derived from a Giessen EDF [28,29] and showed that with these spin-orbit potentials the shell effects are slightly stronger at $Z = 114$ than at $Z = 120$. However, the island of stability is rather flat and looks like an island of coral reef origin due to the interplay between the proton and neutron shell closures.

Compared to Ref. [32], in the present paper more details of calculations and results will be presented to relate the self-consistent and MM approaches. One of our aims is the extraction of the single-particle central and spin-orbit potentials

from the self-consistent nonrelativistic Giessen EDF-plus-HFB theory [28,29] and the comparison of them with those used in the MM approaches [12–14]. In this way one can reveal the reason for the difference between the predictions of these approaches. If the phenomenological MM approach provides a better description of the experimental data, then this comparison can indicate the way to improve the EDF. Another aim is to use these extracted central and spin-orbit potentials in the MM approach and to predict the nuclear properties of SHN with charge numbers $Z = 112$–126. The question is how the spin-orbit interaction affects the center and border of the island of stability and the shape coexistence in SHN. Note that knowledge of the nuclear properties of SHN is important for finding the optimal reactions for their production and the α-decay modes for their identification.

The article is organized as follows. In the next section, the theoretical approach is applied to extract the central and spin-orbit single-particle potentials from the non-relativistic Giessen EDF-plus-HFB theory [28,29]. In Sec. III, the MM approach is briefly introduced. In Sec. IV, the extracted single-particle potentials are used in the MM approach to find the ground-state shell corrections in nuclei with charge numbers $Z = 112$–126 and to determine the region of nuclei with the strongest shell effects. For the SHN, the energy dependencies of the ground-state level-density parameters are calculated with the mean-field potentials extracted from the self-consistent approach (dashed lines) and ones from the MM approach [14]. The shape coexistence in SHN is discussed in relation to its effect on the spectrum of α decay. The one-quasiparticle spectra of SHN in the α-decay chains of $^{295}119$ and $^{295,297,299}120$ are considered to search for isomeric states and possible α-decay energies. The relationship between the effective mass and spin-orbit potential is derived in the Appendix. Finally, we summarize our work in Sec. V.

II. EXTRACTION OF CENTRAL AND SPIN-ORBIT MEAN-FIELD POTENTIALS FROM NONRELATIVISTIC GIESSEN EDF-PLUS-HFB THEORY

The phenomenological central potentials of Wood-Saxon (WS) shape and corresponding spin-orbit potentials with various sets of parameters [12,33–39] are often used in the MM approaches. The parameters are adjusted to known proton and neutron separation energies by assuming an overall mass dependence of the potential radii according to the $A^{1/3}$ law. The shell evolution as reflected by the single-particle energies is then used as the microscopic input, adding, so to speak, quantum fluctuations to the macroscopic bulk of nuclear masses. At the moment it is difficult to test the best WS parametrization for nuclei beyond $Z = 114$ due to insufficient experimental data.

In addition to the phenomenological parametrization, it is possible to extract the single-particle potentials from EDFs, which are suitable for a good description of well-studied nuclei. The transformation of the central and spin-orbit mean-field potentials obtained from the nonrelativistic EDF into the Schrödinger-equivalent single-particle potentials is appropriate for use in the MM method. Thus, the task is to project the density-dependent effective mass contributions from the kinetic operators to the central single-particle potentials, while retaining the essential features of the microscopic self-consistent mean fields [26,27].

In Refs. [28,29], the covariant Lagrangian EDF was constructed in *ab initio* manner by using an interaction energy density obtained from Dirac-Brueckner-Hartree-Fock G matrices in asymmetric nuclear matter. The density-dependent contact pairing interactions in the proton-proton and neutron-neutron channels, respectively, are derived from the Bonn-A NN interaction, leading to state-dependent pairing gaps. The validity of the EDF used here is confirmed by a theoretical analysis and successful descriptions of the data all over the mass table, not only of nuclear ground states but also of spectral properties of stable and exotic nuclei; e.g., see [29,40–43].

Because the proton ($q = Z$) and neutron ($q = N$) self-energies $\Sigma_q(k, \rho)$ are density-dependent [29], there are the renormalization of nucleon masses m_q^* in the HFB approach. As a result, the self-consistent approaches lead to single-particle potentials given in nonrelativistic formulation by

$$U_q(\rho) = V_q(\rho) + V_q^{(ls)}(\rho) = \frac{\hbar^2 k_{\mathrm{F}_q}^2}{2m_q}\left(1 - \frac{m_q}{m_q^*}\right) + \Sigma_q\left(k_{\mathrm{F}_q}, \rho\right) + V_q^{(ls)}(\rho) \quad (1)$$

depending on the nuclear density ρ. Here, k_{F_q} is the wave number at the Fermi surface, m_q is the bare nucleon mass, and $V_q^{(ls)}(\rho)$ is the spin-orbit single-particle potential written here separately from the central single-particle potential $V_q(\rho)$. With a radial-dependent effective mass the equation for the single-particle wave function ψ_q is as follows:

$$\left(-\nabla \cdot \frac{\hbar^2}{2m_q^*(\mathbf{r})}\nabla + V_q(\mathbf{r}) + V_q^{(ls)}(\mathbf{r}) - \varepsilon_q\right)\psi_q(\mathbf{r}) = 0. \quad (2)$$

This equation differs from the Schrödinger equation in the phenomenological approaches because it contains the density-dependent effective mass $m_q^*(\mathbf{r})$. Reducing Eq. (2) to the standard Schrödinger equation as in Refs. [26,27], we obtain

$$\left(-\frac{\hbar^2}{2m_q}\nabla^2 + U_q(r) + U_q^{(ls)}(r) - \varepsilon_q\right)\psi_q(r) = 0, \quad (3)$$

where

$$U_q(r) = V_q(r) + \frac{\hbar^2}{2m_q}\mu_q(r)\bar{k}_{\mathrm{eff}} + \frac{3}{5}\left(1 - \frac{m_q^*(r)}{m_q}\right)\frac{\hbar^2 k_{\mathrm{F}_q}^2(r)}{2m_q^*(r)}. \quad (4)$$

The expressions for $\bar{k}_{\mathrm{eff}}$ and $\mu_q(r)$ are given in Refs. [26,27] as

$$\bar{k}_{\mathrm{eff}} = -\frac{1}{2}\mu_q + \frac{3}{8k_{\mathrm{F}_q}^3}\left[k_{\mathrm{F}_q}\sqrt{\frac{1}{4}\mu_q^2 + k_{\mathrm{F}_q}^2}\left(\frac{1}{4}\mu_q^2 + 2k_{\mathrm{F}_q}^2\right) - \frac{1}{16}\mu_q^4 \mathrm{arcsinh}\left(\frac{2k_{\mathrm{F}_q}}{\mu_q}\right)\right] \quad (5)$$

and

$$\mu_q(r) = \frac{d\ln(m_q^*(r)/m_q)}{dr}.$$

Because of the density dependence of m_q^* in the self-consistent approach, there is a repulsive correction term to the bare self-consistent mean-field potential V_q. So, the Schrödinger-equivalent central mean-field potential U_q is less deep than the potential V_q and has to be compared with the corresponding phenomenological central single-particle potential. With the correction on the self-consistent potential, the Schrödinger-equivalent potential U_q can be regarded as the central potential for the Schrödinger equation with bare nucleon mass.

In Eq. (2), we write separately the spin-orbit potential which arises from the corresponding part of the nonrelativistic EDF. In thenon-relativistic EDF this part, which is defined in terms of the isoscalar and isovector interactions and corresponding spin currents, requires some parameters. However, in the RMF the spin-orbit potential consistently appears and it is strictly related to the difference of scalar S and vector V fields while the central potential $V_q = S + V$ (see the Appendix). Thus, in the RMF theory the central and spin-orbit single-particle self-energies are determined in an unified manner by the same set of scalar and vector fields. The quantity relevant for the spin-orbit potential is the effective mass m_q^*, including the Dirac mass and the sum of scalar and vector Dirac self-energies (plus a minor state-dependent constant energy term) [26,27]. In the nonrelativistic limit m_q^* becomes the effective Schrödinger mass. This allows us to exploit a well-known relation,

$$U_q^{(ls)}(r) = \frac{m_q^*(r)}{m_q} V_q^{(ls)}(r) = -\frac{1}{m_q}\frac{1}{r}\frac{\mathrm{d}\ln(m_q^*(r)/m_q)}{\mathrm{d}r}\mathbf{l}\cdot\mathbf{s}, \qquad (6)$$

of covariant mean-field theory and define the Schrödinger-equivalent spin-orbit mean-field potentials in terms of effective masses derived from the nonrelativistic Giessen EDF [28,29] (Appendix). In Eq. (6), l and s are in the units of $\hbar$. So, the spin-orbit single-particle potentials can be found with Eq. (6) using the dependence of $m_q^*(r)$ on the radial coordinate r. Note that this definition of $U_q^{(ls)}(r)$ in the noncovariant theory differs from the usual practice. As shown for the first time in the Appendix, the relationship between the effective mass and spin-orbit potential imposes a strict correlation between the parameters of the Skyrme EDF.

III. MM APPROACH

The central and spin-orbit single-particle potentials found from the nonrelativistic Giessen EDF-plus-HFB theory are employed in the MM approach [44,45] to find the shell-corrections and the binding energies at the ground states of SHN. The potential energy is calculated as the sum of two terms,

$$U = U_{LDM} + \delta U_{\mathrm{mic}}. \qquad (7)$$

The first term in (7) is a smoothly varying macroscopic energy (the Coulomb and surface energies) calculated with the liquid-drop model. The second term δU_{mic} contains the shell E_{sh} and pairing corrections.

Although the parameters of WS form factors are extracted from the self-consistent model for the spherical nuclei, they are relevant when considering the nuclear deformation in the MM model. The equilibrium deformation of the nucleus corresponds to the position of the corresponding minimum on the potential energy surface U. The calculations account for deformation effects, assuming axial symmetry. The shape of a deformed nucleus is described by a set of multipole parameters β_λ ($\lambda \geqslant 2$). As found, the considered isotopes of nuclei with $Z = 118$–126 are almost spherical while the nuclei with $Z = 112$–116 are slightly deformed with the parameters of quadrupole deformation $\beta_2 \leqslant 0.15$, closely resembling the values predicted in Ref. [14]. For nuclei with $Z < 110$, the absolute values of microscopic corrections obtained in our calculations are close to those obtained in Refs. [12–14]. Also, the description of the single-particle spectra and nucleon density profiles are rather good [27,46,47]. With our MM approach one can calculate the energy Q_α of α decay and structure properties of SHN [25–27,38].

IV. RESULTS AND DISCUSSIONS

For the present large-scale MM calculations, we use the central spin-independent HFB mean-field potentials (4) and effective masses from the nonrelativistic Giessen EDF [26–29]. Employing these effective masses and Eq. (6), we obtain the spin-orbit mean-field potentials. Then the central and spin-orbit single-particle potentials are fitted in a convenient forms and used in the MM approach to find the shell corrections in the ground states of nuclei with $Z = 112$–126.

A. Parametrization of single-particle potentials extracted from nonrelativistic Giessen EDF-plus-HFB theory

1. *Central single-particle potentials*

The central single-particle potentials (isoscalar plus isovector) extracted from the nonrelativistic Giessen EDF-plus-HFB calculations are fitted with the WS form factors [26,27]

$$U_q(r) = \frac{V_q^0}{1 + \exp[(r - R_q)/a_q]},$$

where $V_q^0 = -(58.3 \pm 32\frac{N-Z}{A})$ MeV, $R_q = r_{0q}A^{1/3}$, and $r_{0N} = 1.24$ fm, $r_{0Z} = 1.25$ fm, $a_N = 0.68$ fm, $a_Z = 0.75$ fm for the heavy nuclei considered. Here, the plus and minus signs correspond to $q = Z$ and $q = N$, respectively. The values of r_{0q} obtained are smaller than (close to) those of the phenomenological WS potential in Ref. [14] ([33]). The values of a_q are relatively close in all approaches.

The self-consistent calculations result in 3–11 MeV deeper potential wells than those used in the phenomenological WS parametrizations. For example, in comparison with the WS potential extracted from the self-consistent approach, in the MM model [14] the depth $V_q^0 = -(49.6 \pm 42.66\frac{N-Z}{A})$ MeV of the WS potential used is smaller for the heaviest nuclei. For example, the HFB results in $V_Z^0 = -64.354$ MeV and $V_N^0 = -52.25$ MeV for $^{296}120$, but the values -57.67 and -41.53 MeV, respectively, follow from Ref. [14]. So, the isospin dependence of the mean-field potential is stronger in the MM model [14]. In the expressions $a_{\mathrm{sym}}\frac{(N-Z)^2}{A}$ for the macroscopic symmetry nuclear energy, the coefficient a_{sym} is related to the isospin-asymmetric part V_1 of the potential

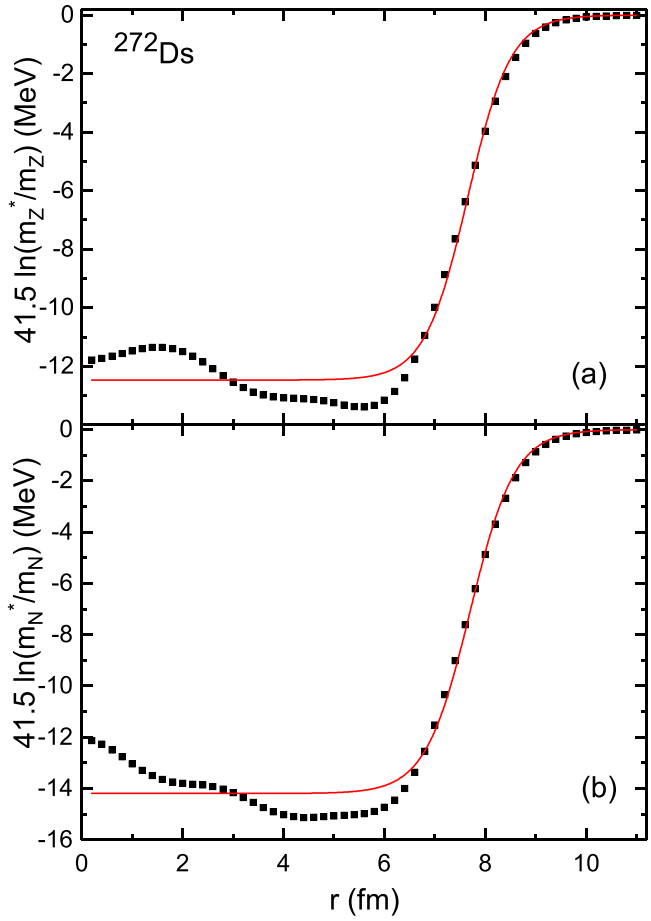

FIG. 1. The calculated values of $41.5\ln(m_q^*(r)/m_q)$ for protons (a) and neutrons (b) of the spherical nucleus ^{272}Ds are shown by symbols. The results of a fit by the WS form factors are shown by solid lines.

depth $V_q^0 = V_0 \pm V_1 \frac{N-Z}{A}$, $V_1 = a_{\rm sym}$ [48]. In the "universal" WS potentials [49] as well as in the WS potentials used in the quasiparticle-phonon model (QPM) [33,34], the value of V_1 is about 40 MeV. If the "universal" WS potentials are used to fit the single-particle spectra for magic nuclei [50], the value of V_1 becomes about 33.6 MeV. The WS potentials with almost the same values of V_1 were suggested in Ref. [35].

2. Spin-orbit single-particle potentials

For spherical nucleus ^{272}Ds, the dependencies of $41.5\ln[m_q^*(r)/m_q]$ on r [see Eq. (6)] are presented in Fig. 1. In spite of the hump at small r, these dependencies are well approximated by the WS form factors. There are similar humps in the central single-particle potentials [26,27] which mainly affect only the states with small orbital quantum numbers l whose wave functions are maximal at small r and which are less important for the shell effects in the heavy nuclei considered. Because the spin-orbit single-particle potential is defined by the derivative of $\ln[m_q^*(r)/m_q]$ with respect to r [see Eq. (6)], it has the largest value near the nuclear surface (at least three times larger that the maximal absolute value of $\frac{d}{dr}\ln[m_q^*(r)/m_q]$ at small r). Shell effects turn out to be most sensitive to the spin-orbit strengths at the nuclear surface.

For the spin-orbit single-particle potentials, we use Eq. (6) in parametrized form as follows:

$$U_q^{(ls)}(r) = -\kappa_q \frac{1}{r}\frac{\rm d}{{\rm d}r}\frac{V_q^0}{1+\exp[(r-R'_q)/a'_q]}\mathbf{l}\cdot\mathbf{s}, \qquad (8)$$

where the constants $\kappa_N = 0.27$ fm^2 and $\kappa_Z = 0.19$ fm^2, $a'_N = 0.46$ fm and $a'_Z = 0.435$ fm, and the radii R'_q are calculated with $r'_{0N} = 1.19$ fm and $r'_{0Z} = 1.18$ fm. As in Ref. [14], the parameters r'_{0q} differ from r_{0q} and $r'_{0q} < r_{0q}$. However, $a'_q < a_q$ in our case, that also follows from the RMF calculations in Ref. [26]. Indeed, the sum and difference of scalar and vector potentials result in the differences of r_{0q} and a_q from r'_{0q} and a'_q, respectively. As follows from Eq. (8), the spin-orbit strength is proportional to κ_q/a'_q: the smaller the effective mass in the center of nucleus and the smaller the diffuseness a'_q, the stronger the spin-orbit potential. So, the spin-orbit potential is strongly related to the function $m_q^*(r)$.

B. Level-density parameters of SHN

In comparison with the phenomenological approach the self-consistent ones result in a deeper central mean-field potentials. The deeper potential well leads to smaller level density near the Fermi surface and could change the shell correction to the binding energy. The level-density parameters a are calculated as in Ref. [51]. In Fig. 2, they are compared with those obtained for shallower potential well used in Ref. [14]. As seen, the deeper potential well results in smaller a by about 15%. So, in the calculation of the survival probabilities for SHN the value of level-density parameter should be consistent with the mean-field potentials used.

C. Quasiparticle levels

One-quasiparticle levels are calculated with the superfluid nuclear model using the variation principle and single-particle states in the extracted mean-field potentials at equilibrium deformation parameters β_2 and β_4. The blocking effect is taken into consideration. The one-quasiparticle energies are strongly affected not only by the mean-field single-particle levels, but by the residual pairing and quasiparticle-phonon interactions. These interactions are taken into consideration with the quasiparticle phonon model [33,34]. In the calculations, the quadrupole and octupole phonons are taken into account.

1. Actinides

To evaluate the quality of the description of one-quasiparticle spectra with the mean-field potential extracted from the self-consistent consideration, we compare the calculated spectra for ^{243}Cm, ^{251}Cf, ^{247}Bk, and ^{251}Es with the available experimental data [52] and those obtained with the phenomenological WS potential (Figs. 3 and 4). The phenomenological WS potentials [38,44] with $V_q^0 = -[54.25 \pm 39.6(N-Z)/A]$ MeV, $r_{0N} = 1.26$ fm, $r_{0Z} = 1.24$ fm, $a_N = a'_N = 0.74$ fm, $a_Z = a'_Z = 0.645$ fm, $\kappa_N = 0.45$, and $\kappa_Z = 0.32$ were adopted for the best description of the low-lying

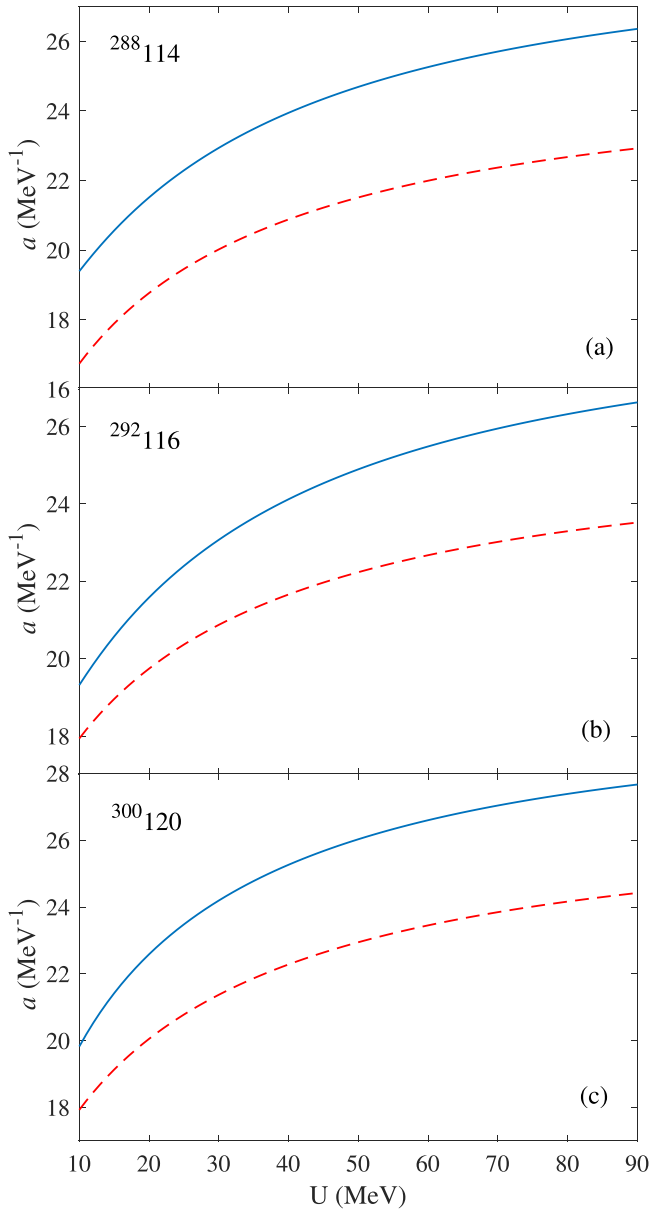

FIG. 2. Energy dependencies of the ground-state level-density parameters calculated with the mean-field potentials extracted from the self-consistent approach (dashed lines) and the ones from Ref. [14] (solid lines) for nuclei ^{288}Fl (a), ^{292}Lv (b), and ^{300}120 (c).

quasiparticle states. The potential for protons (neutrons) is about 3 MeV (6 MeV) shallower. While $a_N < a_Z$ in our case, in the phenomenological WS potential $a_N > a_Z$. As seen in Figs. 3 and 4, the phenomenological WS potentials result in a better description of the experimental data. However, the mean-field potentials extracted from the self-consistent approach provide quite a satisfactory description of one-quasiparticle spectra. The same conclusion was also reached in Ref. [30].

2. *SHN of α-decay chains with* ^{295}119 *and* ^{295,297,299}120

The one-quasiparticle spectra of odd-mass nuclei with $Z = 119$ and 120, which can be produced in complete fusion

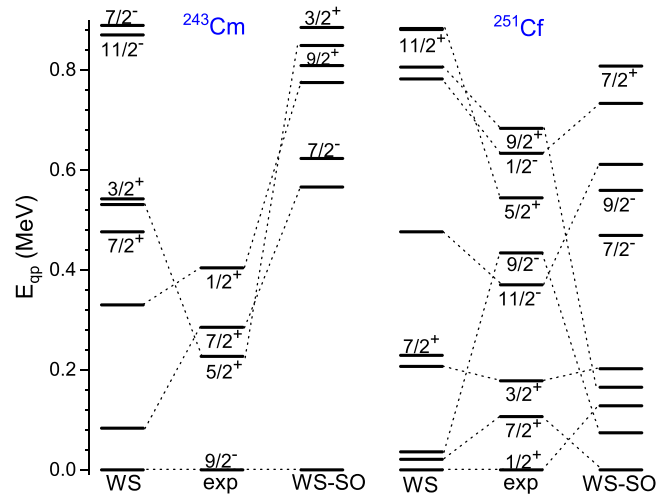

FIG. 3. Calculated energies of low-lying one-quasineutron states (WS-SO) in ^{243}Cm and ^{251}Cf are compared with the available experimental data [52] and those (WS) obtained with the phenomenological WS potentials (see text).

reactions, are of special interest. In Fig. 5, the calculated one-quasiproton spectra and α decays from the ground and possible isomeric states are shown in the nuclei of the α-decay chain of the ^{295}119 nucleus. As seen in Fig. 5, the values of Q_α in ^{279}Rg, ^{283}Nh, and ^{287}Mc are reproduced well. Note that the calculated Q_α values in even-even SHN are also in a good agreement with the experimental data. For example, for the α decay of the nuclei ^{284}Cn, ^{288}Fl, and ^{292}Lv we obtain $Q_\alpha = 9.87$, 10.18, and 10.64 MeV, respectively, while the experimental values are 9.60, 10.07, and 10.776 MeV [3,53].

Definition of the spin-orbit interaction different from [45] leads here to some changes of the ground-state deformations and order of one-quasiparticle states. As in Ref. [45], there is low-lying isomeric state $1/2^-[510]$ in ^{295}119, and two α-decay lines are possible in this nucleus (Fig. 5). The obtained difference of Q_α results in about two orders of magnitude different half-lives. However, the α decay of ^{291}Ts is less

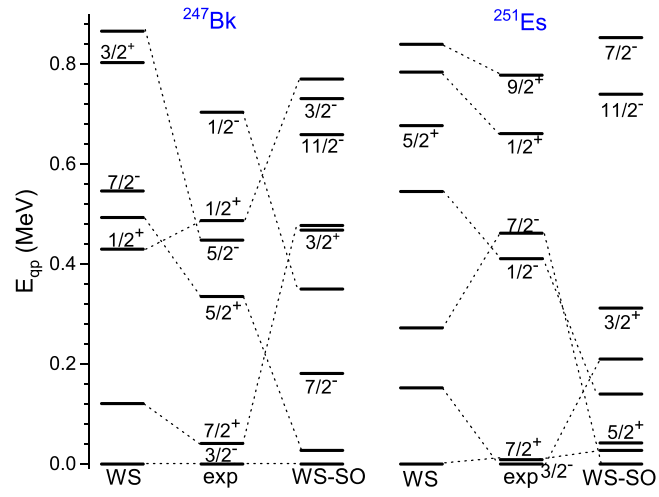

FIG. 4. The same as in Fig. 3, but for one-quasiproton states in ^{247}Bk and ^{251}Es.

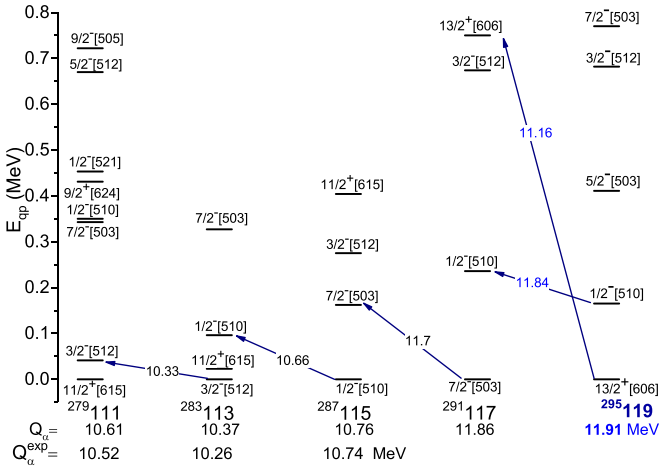

FIG. 5. Calculated energies of low-lying one-quasiproton states in the indicated nuclei of the α-decay chain of $^{295}119$. The calculated values of Q_α are for the ground-state-to-ground-state α decays. The α decays with $\Delta K = 0$ and $\Delta K \neq 0$ are traced by solid and dashed arrows, respectively. The experimental values of $Q_\alpha^{\rm exp}$ are from Refs. [1,3].

hindered in the present calculation. One can also see the stronger shell effects in ^{283}Nh than those in Ref. [45].

The possible α-decay chain of $^{295}120$ nucleus is presented in Fig. 6. In comparison to the results of Ref. [45], the α-decay from the ground state is unhindered The α decay from the isomeric state $15/2^-[707]$ in $^{295}120$ occurs if this state lives longer than 0.3 ms, which is unlikely taking into account its position at 0.72 MeV and coupling with other states. The α decay of $^{295}120$ with $Q_\alpha = 12.22$ MeV likely occurs in $T_\alpha \approx 0.8$ ms, that is much shorter than the expected half-life 0.1 s for spontaneous fission [54]. As in Ref. [45], the interruption of the α-decay chain in Fig. 6 is expected below ^{279}Cn.

As seen in Figs. 6 and 7, there are stronger shell effects when the neutron number approaches $N = 174$ (the deformed neutron subshell). The α decay of $^{297}120$ is hindered because the state $1/2^+[620]$ in ^{293}Og has energy larger than 0.8 MeV.

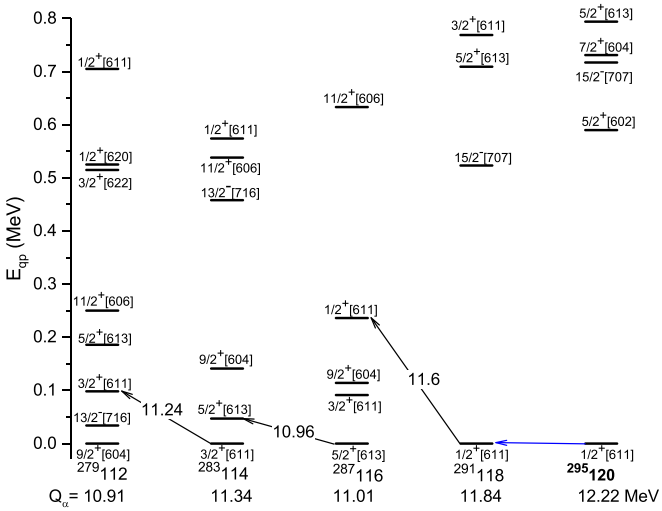

FIG. 6. The same as in Fig. 5, but for the α-decay chain of $^{295}120$.

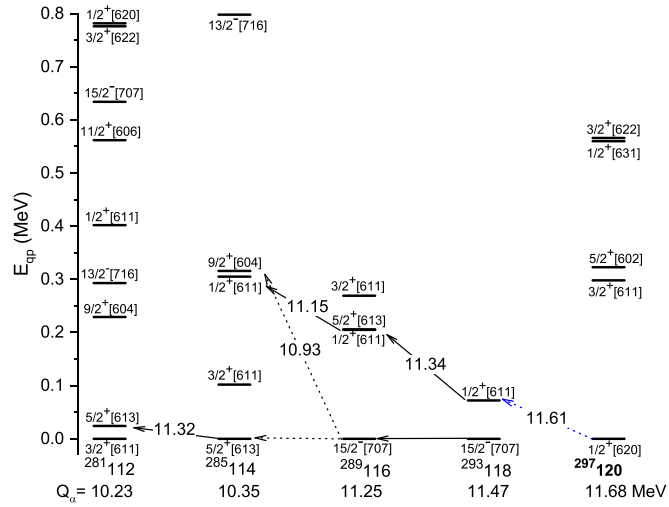

FIG. 7. The same as in Fig. 5, but for the α-decay chain of $^{297}120$.

The isomeric $1/2^+[611]$ state of ^{293}Og is likely populated in the α decay of $^{297}120$. So, the α decay of ^{293}Og can be delayed or have two lines in Fig. 7. As in Ref. [45], the α decay from the ground state of ^{289}Lv is strongly hindered. The α decay can also occur from the isomeric state $1/2^+[611]$ ^{289}Lv if it lives longer than 15 ms. The interruption of α-decay chain in Fig. 7 is expected below ^{285}Fl.

The possible α-decay chain of $^{299}120$ is presented in Fig. 8. As seen, the α decays of $^{299}120$ and ^{295}Og are hindered because of the positions of corresponding states in the parent nuclei. For example, the α decay of ^{295}Og likely occurs to the ground state $1/2^+[611]$ of ^{291}Lv because the state $1/2^+[620]$ is located at the much higher energy at 1.27 MeV. The variation of ground-state deformations ($\beta_2 = 0.019$, 0.1, and 0.136 for $^{299}120$, ^{291}Lv, and ^{287}Fl, respectively) leads to the same quantum numbers for the ground states of these nuclei.

As found, in $^{296,298,300}120$ the two-quasiparticle isomeric states with $K > 4$ have energies larger than 1 MeV. The lowest two-quasiproton $9^-_\pi(13/2^+[606] \otimes 5/2^-[503])$ isomeric state

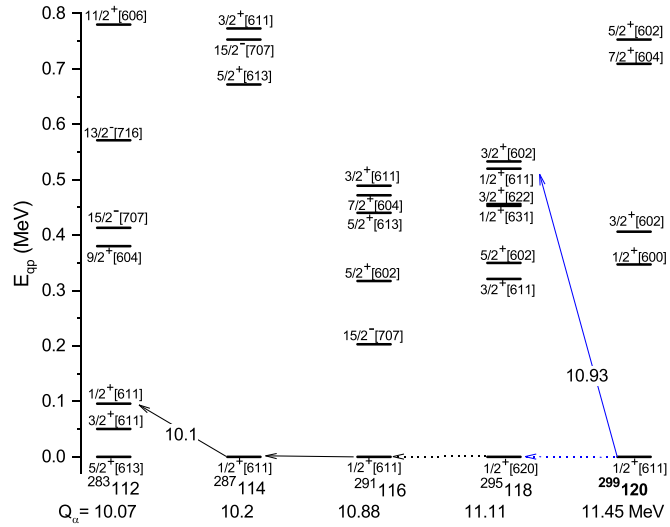

FIG. 8. The same as in Fig. 5, but for the α-decay chain of $^{299}120$.

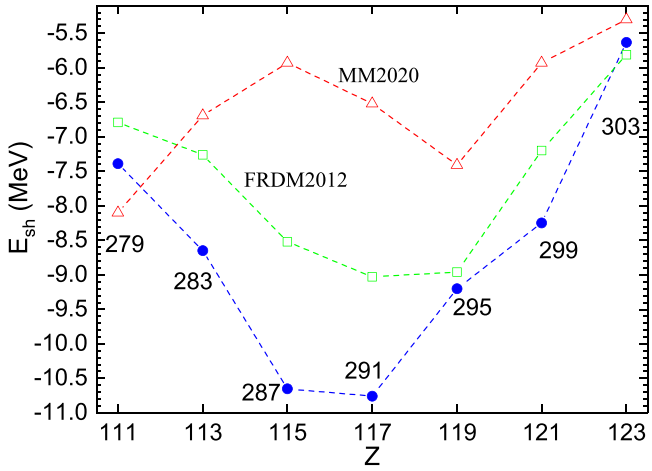

FIG. 9. The calculated ground-state shell correction energies in nuclei of the α-decay chain containing $^{295}119$. Our results (closed circles) obtained with the MM method using the self-consistent mean-field potentials are compared to the microscopic corrections from the FRDM2012 [12] (open squares) and MM2020 [14] (open triangles) The lines are drown to guide the eye.

is in $^{296}120$ at 1.065 MeV. In ^{292}Og, the state 9^-_π is at energy 1.226 MeV. The α decay to this state occurs if the isomeric 9^-_π state in $^{296}120$ lives longer than 6 ms.

D. Shell effects in α-decay chains with $Z = 119$ and 120 nuclei

The crucial link between the microscopic and macroscopic approaches to nuclear structure is the shell correction energy [55]. Using the central and spin-orbit mean-field potentials extracted here from the self-consistent approach, in addition to Ref. [32] we calculate the ground-state shell corrections for the nuclei of α-decay chains containing the SHN $^{295}119$ and $^{295-297,299,301,304}120$ (Figs. 9–11). In comparison to Ref. [26] where the spin-orbit potentials were partially introduced phenomenologically, the present spin-orbit potentials lead to a slightly larger proton shell at $Z = 114$ than that at $Z = 120$. The maximum difference of proton shell corrections in the considered nuclei with $Z = 114$ and $Z = 120$ reaches about 1 MeV. The interplay between the proton and neutron shell effects results in rather weak dependence of E_{sh} in the range of $Z = 114$–120. In the case of smaller isospin $N - Z$, the deformed neutron shell at $N = 174$ smoothes out the

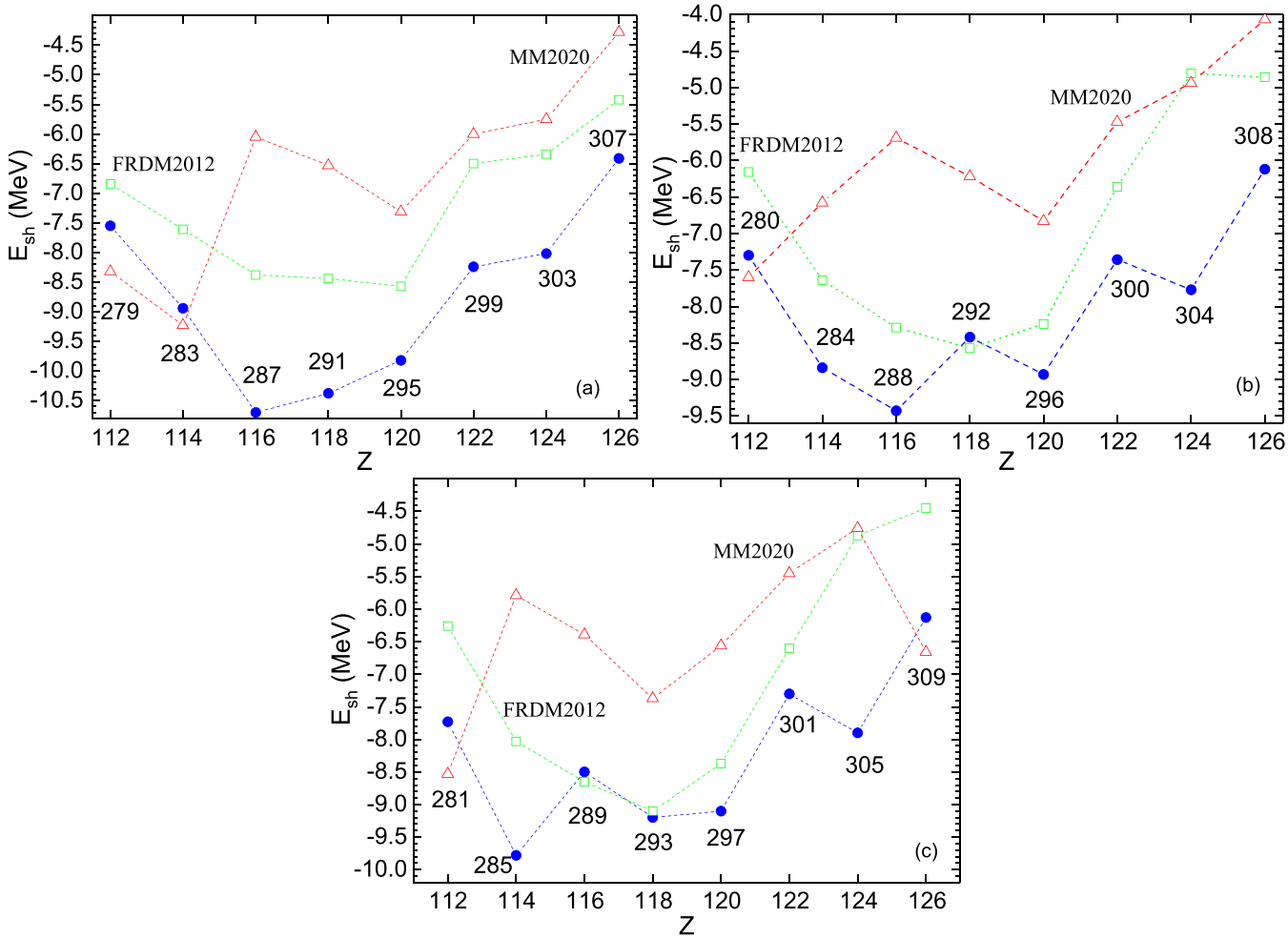

FIG. 10. The same as in Fig. 9, but for nuclei of α-decay chains containing $^{295}120$ (a), $^{296}120$ (b), and $^{297}120$ (c).

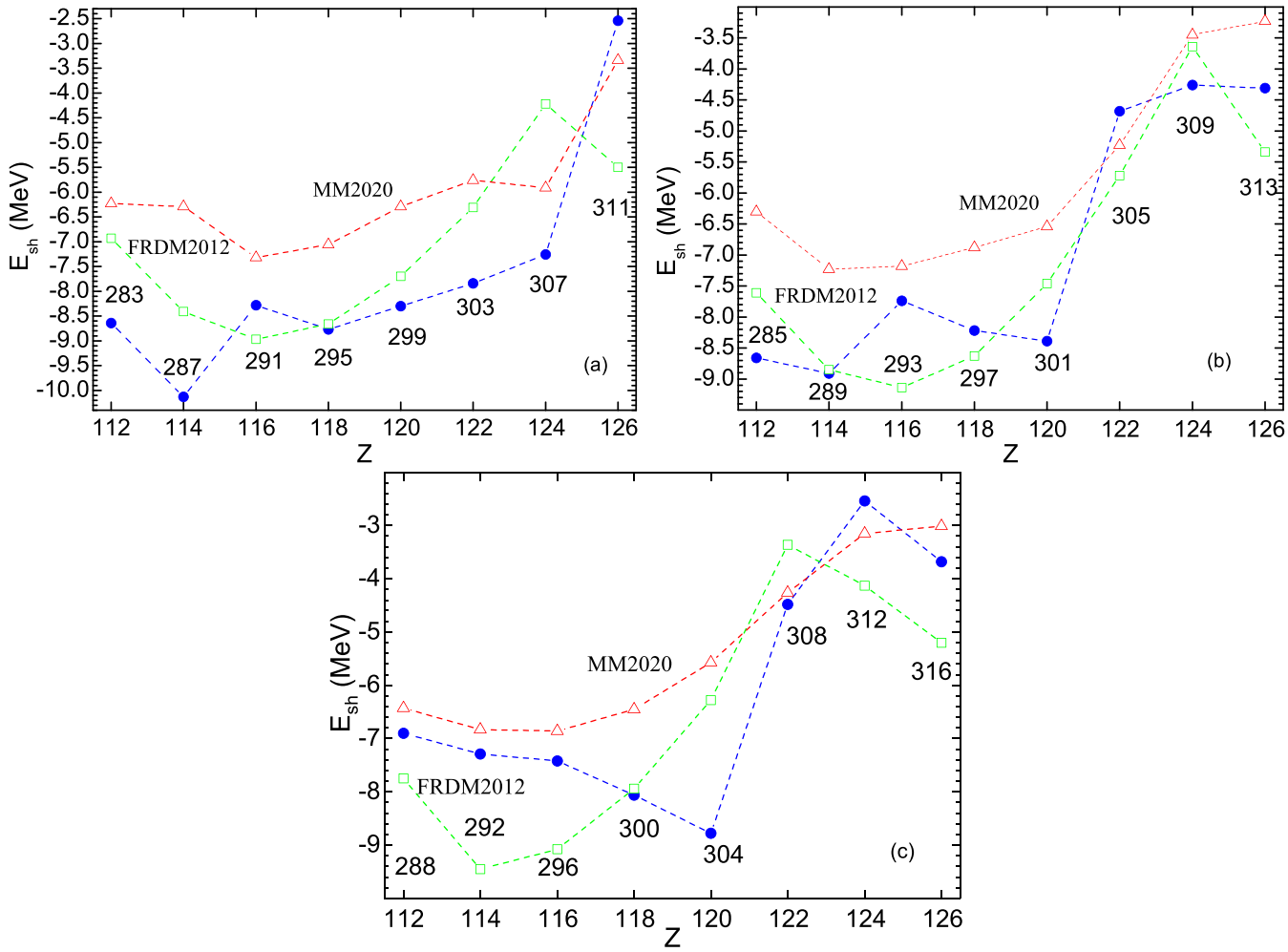

FIG. 11. The same as in Fig. 9, but for nuclei of α-decay chains containing $^{299}120$ (a), $^{301}120$ (b), and $^{304}120$ (c).

dependence of E_{sh} on Z from 114 till 120 and shifts the minimum of E_{sh} to $Z = 116$. In the α-decay chains with larger $N - Z$, the spherical neutron shell at $N = 184$ increases the shell effect at $Z = 120$ and the dependence of E_{sh} on Z remains rather flat. The shell effects were 1–2 MeV stronger at $Z = 120$ in Ref. [26], while the present calculations lead to rather close values of E_{sh} for nuclei with $Z = 114$–120. Because the phenomenological $U_q^{(ls)}(r)$ in Ref. [26] are weaker (smaller κ_q/a'_q) by about 15% than the one used in the present calculations [$U_q(r)$ are the same], one can conclude that minor change of the spin-orbit potentials can shift the minimum of the shell correction energy from $Z = 114$ to $Z = 120$.

For comparison, in Figs. 9–11 we present the microscopic corrections obtained with the FRDM2012 [12] and MM2020 [14] models. Overall, there is a qualitative agreement on the evolution of $E_{sh}(Z, N)$ over whole range from $Z = 112$ to $Z = 126$. The FRDM2012 model results are slightly closer to ours. A common feature of the three approaches, including the present one, is the rapid decrease of shell effects and accordingly of the nuclear stability beyond $Z = 120$. Based on the calculations presented, we expect enhanced shell effects at ($Z = 120, N = 184$), while in Refs. [12,14] ($Z = 114$, $N = 184$) is favored.

In the MM models [25,38,45], the phenomenological single-particle potentials result in the increase of the shell effects toward $Z = 120$ nucleus. However, the shell effects in nuclei with $Z = 114$–118 remain quite large. So, there are certain intervals of parameter values of the phenomenological mean-field potentials in the MM approaches which endorse the stronger shell effects at $Z = 120$ rather than at $Z = 114$. Note that in Refs. [25,38,45] the spin-orbit single-particle potentials were phenomenologically adjusted for a better description of nuclear structure of well studied heavy nuclei. As shown below, the description of these nuclei with the spin-orbit potentials obtained here remains satisfactory.

In all MM approaches considered, including the present one and that in Refs. [25,38,45], the competition between proton and neutron shell effects at $Z = 114$–120 acts like a stabilization effect, inducing a rather weak dependence of E_{sh} on the charge number Z. So, these approaches predict that the island of stability is more like an island of coral reef origin than a volcanic one. This landscape of the island of stability is also supported by the experiment. Indeed, no discontinuity in Q_α and lifetimes was observed in nuclei beyond Fl [1–3].

Note that the MM approaches mentioned describe well the known energies of α decays and, thus, the binding energies.

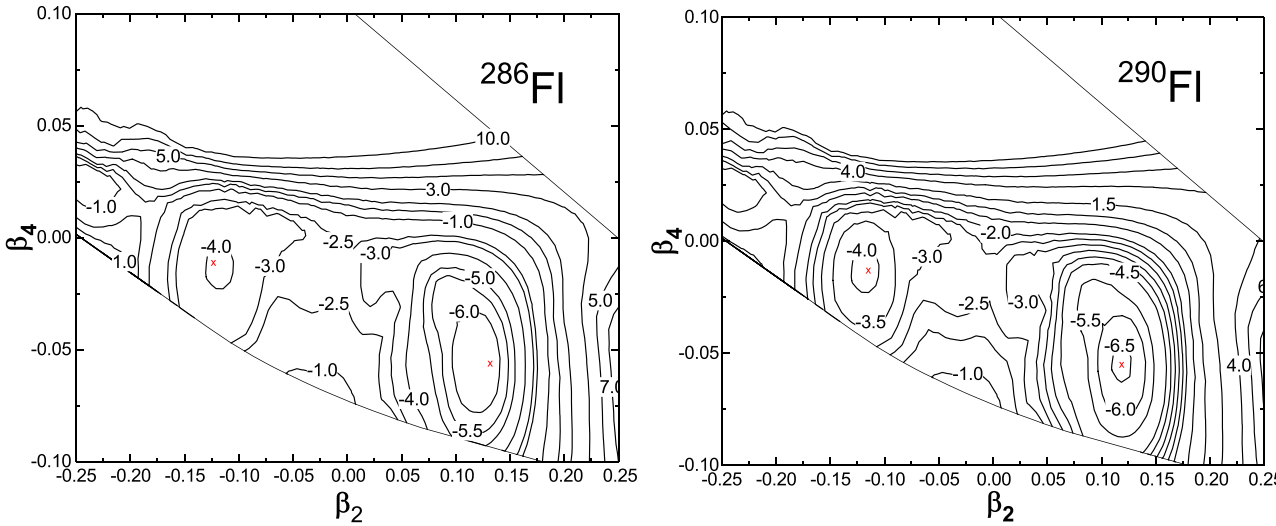

FIG. 12. Contour plots of the potential energy of ^{286,290}Fl as functions of quadrupole β_2 and hexadecupole β_4 deformation parameters. The energies are counted from the potential energy of the corresponding spherical nucleus. The potential minima are marked by crosses. The potential minima at positive β_2 are about 2.5 MeV deeper than those at $\beta_2 < 0$.

Also the self-consistent approaches are suitable to explain the experimental data. The strong difference in the results is obtained only for nuclei beyond Og. Therefore, only future experimental results could indicate the most reliable approach.

E. Shape coexistence in SHN

In nuclei with $Z = 114$–120, the potential energy surfaces as functions of β_2 are rather flat near the ground states and have minima at positive and negative β_2 [38,56]. For example, in Fig. 12 for ^{286,290}Fl there are two minima which differ in energy by approximately 2.5 MeV and are at opposite signs of quadrupole deformations. The deeper minima with the largest $|E_{sh}|$ corresponds to the ground state. For ^{296}120, the minima are at almost the same energy (Fig. 13). With increasing N towards 184, two minima almost coincide and the nucleus becomes spherical (see the case of ^{300}120). So, the shape coexistence phenomenon in SHN is well seen in our axial calculations. The depths and positions of the potential minima depend on the spin-orbit potential used. In comparison to the present calculations, the potential minimum at negative β_2 is deeper in Ref. [38]. If two potential minima are close in energy, the α decays to the states with the same quantum numbers but built in different minima could have different energies. This effect can create an additional line in the spectrum of α particles emitted.

V. SUMMARY

The central and spin-orbit mean-field potentials were extracted from the self-consistent nonrelativistic Giessen

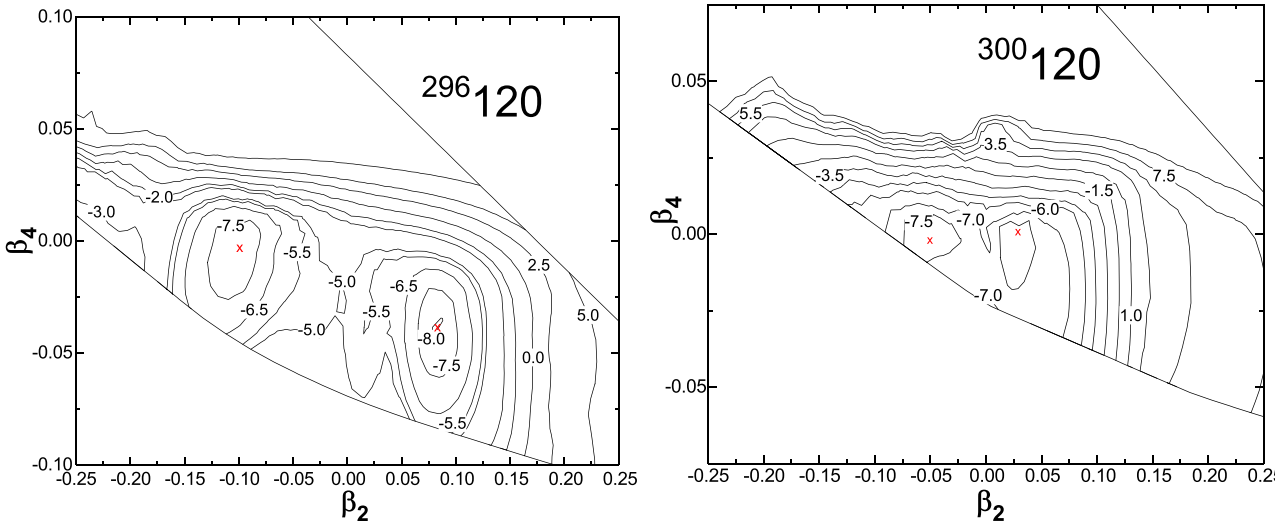

FIG. 13. The same as in Fig. 12, but for nuclei ^{296,300}120. The potential minima at positive β_2 are only about 0.1 MeV deeper than those at $\beta_2 < 0$.

EDF-plus-HFB theory [29]. Special attention was paid to constraining the mean-field spin-orbit potentials by exploiting a well-known relation of covariant mean-field theory. As found, the noncovariant self-consistent approach provides deeper central single-particle potentials than those used in the known MM models [12,14]. The spin-orbit single-particle potentials extracted appear to be of a form like those in phenomenological studies, with comparable strength constant but smaller diffuseness and radius parameters.

The single-particle spectra in SHN are rather dense, and small change of spin-orbit strength leads to important consequences. We revealed that the spin-orbit strengths mainly define the position of the proton shell closure in SHN. As shown, 15% stronger spin-orbit interaction can shift the proton shell from $Z = 120$ to $Z = 114$. Because the position of proton shell closure in SHN is very sensitive to the spin-orbit strength, its experimental indication will allow us to correct the radial dependencies of nucleon effective masses.

To relate the self-consistent and MM approaches, the extracted microscopic mean-field potentials were used in the MM method for calculating the shell correction energies in the nuclei of α-decay chains containing SHN $^{295}119$ and $^{295–297,299,301,304}120$. With these mean-field potentials we obtained quite strong shell effects in nuclei with $Z = 114$–120 due to the interplay between the proton shells at $Z = 114$ and 120 and neutron shells at $N = 174$ and 184, respectively. A central result obtained is the influence of the neutron shell structure on the position of the next double magic nucleus after ^{208}Pb. The shift of the proton shell closure from $Z = 114$ to $Z = 120$ was clearly seen with increasing the neutron number from $N = 174$ to $N = 184$. As in Refs. [12,14], the nuclei are expected to be quite unstable beyond $Z = 120$. Thus, the island of stability looks like an island of coral reef origin with the border $Z = 114$–120 and $N = 174$–184. This prediction of the border supports the attempt to produce nuclei with $Z = 119$ and 120 and to check if they belong to the main reef of the island of stability.

The singe-particle potentials extracted from the self-consistent approach were used to calculate the α-decay energies and one-quasiparticle spectra in actinides and SHN of α-decay chains containing $^{295}119$ and $^{295,297,299}120$. One can conclude from our work that the approaches, which describe well the structure of actinides, indicate quite strong shell effects at $Z = 120$. Another conclusion is that spin-orbit interaction affects the shape coexistence and, correspondingly, the spectrum of α decay in the SHN, for example, in ^{286,290}Fl and $^{296,300}120$. The isomeric states (i.e., $1/2^+[611]$ in ^{289}Lv, $1/2^+[611]$ in ^{293}Og, $1/2^-[510]$ in $^{295}119$, $15/2^-[707]$ in $^{295}120$, and $9^-_\pi(13/2^+[606] \otimes 5/2^-[503])$ in $^{296}120$) and expected α-decay energies in the SHN and the interruptions of α-decay chains were predicted. These results seem to be important for analyzing the experimental spectra of α decay.

From the comparison with available experimental data, we conclude that the Giessen EDF used in the paper is good enough to describe nuclear properties and can serve as a basis for further improvement. Because of the relationship established between the self-consistent and MM approaches, perhaps the EDF can be modified to result in mean-field central and spin-orbit potentials close to those in the successful phenomenological models.

ACKNOWLEDGMENTS

L.A.M., G.G.A., and N.V.A. were supported by Ministry of Science and Higher Education of the Russian Federation (Contract No. 075-10-2020-117). This work was supported in part by the DFG (Bonn, Grant No. Le439/16-2).

APPENDIX

In the Skyrme mean-field Hamiltonian for symmetric nuclear matter [$m^*_q(r) = m^*(r)$, $m_q = m$, and $V^{(ls)}_q = V^{(ls)}$] with density $\rho(r)$ [57,58],

$$m^*(r) = \left(\frac{1}{m} + \frac{3t_1 + (5 + 4x_2)t_2}{8}\rho(r)\right)^{-1} \tag{A1}$$

and

$$V^{(ls)}_{\rm Sk}(r) = \frac{3}{4}W_0\frac{1}{r}\frac{d\rho(r)}{dr}\mathbf{l}\cdot\mathbf{s} \tag{A2}$$

are the effective mass and spin-orbit potential, respectively. Here, t_i $(i = 1, 2)$, x_2, and W_0 are the parameters used in the Skyrme EDF.

In the RMF, the projection onto the upper component of the Dirac function results in the Schrödinger equation [15] with the effective mass (in units $\hbar = c = 1$)

$$m^* = m - \tfrac{1}{2}[V - S] \tag{A3}$$

and the spin-orbit term

$$V^{(ls)} = \frac{1}{(2m)^2}(\nabla v_{ls})\cdot(\mathbf{p}\times\sigma), \tag{A4}$$

where

$$v^{(ls)} = \frac{m}{m^*}[V - S] = \frac{2m}{m^*}(m - m^*). \tag{A5}$$

In the case of spherical symmetry, the spin-orbit term has the well-known form

$$\begin{aligned} V^{(ls)}(r) &= \frac{1}{2m^2}\frac{1}{r}\frac{dv_{ls}(r)}{dr}\mathbf{l}\cdot\mathbf{s} \\ &= \frac{1}{r}\frac{d(m^*(r))^{-1}}{dr}\mathbf{l}\cdot\mathbf{s}. \end{aligned} \tag{A6}$$

Equating the Skyrme and RMF effective masses and spin-orbital potentials

$$V^{(ls)}_{\rm Sk}(r) = V^{(ls)}(r), \tag{A7}$$

we obtain the relationship

$$W_0 = \tfrac{1}{6}[3t_1 + (5 + 4x_2)t_2] \tag{A8}$$

between the constants of the Skyrme Hamiltonian. Equation (A8) can be also written as

$$\frac{3}{4}W_0\rho(r) = \frac{3t_1 + (5 + 4x_2)t_2}{8}\rho(r) = \frac{1}{m^*} - \frac{1}{m}. \tag{A9}$$

Thus, we reduce the number of constants and obtain the Skyrme spin-orbit potential in the form of Eq. (A6).

Equation (A9) results in a strong correlation between the value of W_0 and the parameters t_1, t_2, and x_2. For SkM*

[59], SLy4 [60], and T43 [61] parametrizations of EDF, $W_0 = 130$, 123, and 153.103 MeV fm^5, respectively, while Eq. (A9) leads to $W_0 = 92.5$, 152.35, and 144 MeV fm^5, respectively.

[1] Yu. Ts. Oganessian, J. Phys. G **34**, R165 (2007).

[2] Y. T. Oganessian, F. S. Abdullin, P. D. Bailey, D. E. Benker, M. E. Bennett, S. N. Dmitriev, J. G. Ezold, J. H. Hamilton, R. A. Henderson, M. G. Itkis, Y. V. Lobanov, A. N. Mezentsev, K. J. Moody, S. L. Nelson, A. N. Polyakov, C. E. Porter, A. V. Ramayya, F. D. Riley, J. B. Roberto, M. A. Ryabinin, K. P. Rykaczewski, R. N. Sagaidak, D. A. Shaughnessy, I. V. Shirokovsky, M. A. Stoyer, V. G. Subbotin, R. Sudowe, A. M. Sukhov, Y. S. Tsyganov, V. K. Utyonkov, A. A. Voinov, G. K. Vostokin, and P. A. Wilk, Phys. Rev. Lett. **104**, 142502 (2010); Phys. Rev. C **87**, 014302 (2013); **87**, 034605 (2013); **87**, 054621 (2013); V. K. Utyonkov, N. T. Brewer, Y. T. Oganessian, K. P. Rykaczewski, F. S. Abdullin, S. N. Dmitriev, R. K. Grzywacz, M. G. Itkis, K. Miernik, A. N. Polyakov, J. B. Roberto, R. N. Sagaidak, I. V. Shirokovsky, M. V. Shumeiko, Y. S. Tsyganov, A. A. Voinov, V. G. Subbotin, A. M. Sukhov, A. V. Sabelnikov, G. K. Vostokin, J. H. Hamilton, M. A. Stoyer, and S. Y. Strauss, *ibid.* **92**, 034609 (2015).

[3] Yu. Ts. Oganessian and V. K. Utyonkov, Nucl. Phys. A **944**, 62 (2015); Rep. Prog. Phys. **78**, 036301 (2015).

[4] R. Eichler *et al.*, Nature (London) **447**, 72 (2007).

[5] S. Hofmann *et al.*, Eur. Phys. J. A **32**, 251 (2007).

[6] L. Stavsetra, K. E. Gregorich, J. Dvorak, P. A. Ellison, I. Dragojevic, M. A. Garcia, and H. Nitsche, Phys. Rev. Lett. **103**, 132502 (2009).

[7] C. E. Dullmann, M. Schadel, A. Yakushev, A. Turler, K. Eberhardt, J. V. Kratz, D. Ackermann, L. L. Andersson, M. Block, W. Bruchle, J. Dvorak, H. G. Essel, P. A. Ellison, J. Even, J. M. Gates, A. Gorshkov, R. Graeger, K. E. Gregorich, W. Hartmann, R. D. Herzberg, F. P. Hessberger, D. Hild, A. Hubner, E. Jager, J. Khuyagbaatar, B. Kindler, J. Krier, N. Kurz, S. Lahiri, D. Liebe, B. Lommel, M. Maiti, H. Nitsche, J. P. Omtvedt, E. Parr, D. Rudolph, J. Runke, B. Schausten, E. Schimpf, A. Semchenkov, J. Steiner, P. Thorle-Pospiech, J. Uusitalo, M. Wegrzecki, and N. Wiehl, Phys. Rev. Lett. **104**, 252701 (2010).

[8] J. M. Gates, C. E. Dullmann, M. Schadel, A. Yakushev, A. Turler, K. Eberhardt, J. V. Kratz, D. Ackermann, L. L. Andersson, M. Block, W. Bruchle, J. Dvorak, H. G. Essel, P. A. Ellison, J. Even, U. Forsberg, J. Gellanki, A. Gorshkov, R. Graeger, K. E. Gregorich, W. Hartmann, R. D. Herzberg, F. P. Hessberger, D. Hild, A. Hubner, E. Jager, J. Khuyagbaatar, B. Kindler, J. Krier, N. Kurz, S. Lahiri, D. Liebe, B. Lommel, M. Maiti, H. Nitsche, J. P. Omtvedt, E. Parr, D. Rudolph, J. Runke, H. Schaffner, B. Schausten, E. Schimpf, A. Semchenkov, J. Steiner, P. Thorle-Pospiech, J. Uusitalo, M. Wegrzecki, and N. Wiehl, Phys. Rev. C **83**, 054618 (2011).

[9] S. Hofmann *et al.*, Eur. Phys. J. A **48**, 62 (2012).

[10] J. M. Khuyagbaatar *et al.*, Phys. Rev. Lett. **112**, 172501 (2014).

[11] S. Hofmann *et al.*, Eur. Phys. J. A **52**, 180 (2016).

[12] P. Möller, A. J. Sierk, T. Ichikawa, and H. Sagawa, At. Data Nucl. Data Tables **109-110**, 1 (2016); http://t2.lanl.gov/nis/data/astro/molnix96/molnix.html

[13] I. Muntian, Z. Patyk, and A. Sobiczewski, Acta. Phys. Pol. B **32**, 691 (2001); **34**, 2141 (2003); I. Muntian, S. Hofmann, Z. Patyk, and A. Sobiczewski, *ibid.* **34**, 2073 (2003); Phys. At. Nucl. **66**, 1015 (2003); A. Parkhomenko, I. Muntian, Z. Patyk, and A. Sobiczewski, Acta. Phys. Pol. B **34**, 2153 (2003); A. Parkhomenko and A. Sobiczewski, *ibid.* **36**, 3095 (2005).

[14] P. Jachimowicz, M. Kowal, and J. Skalski, At. Data Nucl. Data Tables **138**, 101393 (2021).

[15] P. Ring, Prog. Part. Nucl. Phys. **37**, 193 (1996).

[16] M. Bender, P.-H. Heenen, and P.-G. Reinhard, Rev. Mod. Phys. **75**, 121 (2003).

[17] S. A. Fayans, S. V. Tolokonnikov, E. L. Trykov, and D. Zawischa, Nucl. Phys. A **676**, 49 (2000).

[18] M. Baldo, P. Schuck, and X. Viñas, Phys. Lett. B **663**, 390 (2008).

[19] G. A. Lalazissis, D. Vretenar, and P. Ring, Phys. Rev. C **57**, 2294 (1998).

[20] S.-G. Zhou, J. Meng, and P. Ring, Phys. Rev. C **68**, 034323 (2003).

[21] D. Vretenar, A. V. Afanasjev, G. A. Lalazissis, and P. Ring, Phys. Rep. **409**, 101 (2005).

[22] J. Meng and S.-G. Zhou, J. Phys. G **42**, 093101 (2015).

[23] G. G. Adamian, N. V. Antonenko, and W. Scheid, Phys. Rev. C **81**, 024320 (2010); G. G. Adamian, N. V. Antonenko, S. N. Kuklin, and W. Scheid, *ibid.* **82**, 054304 (2010).

[24] G. G. Adamian, N. V. Antonenko, S. N. Kuklin, B. N. Lu, L. A. Malov, and S. G. Zhou, Phys. Rev. C **84**, 024324 (2011).

[25] A. N. Kuzmina, G. G. Adamian, N. V. Antonenko, and W. Scheid, Phys. Rev. C **85**, 014319 (2012).

[26] G. G. Adamian, L. A. Malov, N. V. Antonenko, H. Lenske, K. Wang, and S. G. Zhou, Eur. Phys. J. A **54**, 170 (2018).

[27] G. G. Adamian, N. V. Antonenko, H. Lenske, L. A. Malov, and S. G. Zhou, Eur. Phys. J. A **57**, 89 (2021).

[28] H. Lenske and C. Fuchs, Phys. Lett. B **345**, 355 (1995).

[29] F. Hofmann and H. Lenske, Phys. Rev. C **57**, 2281 (1998).

[30] A. Bhagwat, M. Centelles, X. Viñas, and P. Schuck, Phys. Rev. C **103**, 024321 (2021).

[31] A. Bhagwat, M. Centelles, X. Viñas, and P. Schuck, Phys. Rev. C **103**, 024320 (2021).

[32] L. A. Malov, G. G. Adamian, N. V. Antonenko, and H. Lenske, Phys. Rev. C **104**, L011304 (2021).

[33] V. G. Soloviev, *Theory of Complex Nuclei* (Pergamon Press, Oxford, 1976).

[34] S. P. Ivanova, A. L. Komov, L. A. Malov, and V. G. Soloviev, Phys. Part. Nucl. **7**, 450 (1976).

[35] V. V. Pashkevich and A. Ya. Rusanov, Nucl. Phys. A **810**, 77 (2008).

[36] Z.-Y. Wu, C. Qi, R. Wyss, and H.-L. Liu, Phys. Rev. C **92**, 024306 (2015).

[37] F. R. Xu, P. M. Walker, and R. Wyss, Phys. Rev. C **59**, 731 (1999).

[38] G. G. Adamian, L. A. Malov, N. V. Antonenko, and R. V. Jolos, Phys. Rev. C **97**, 034308 (2018).

[39] A. Sobiczewski and K. Pomorski, Prog. Part. Nucl. Phys. **58**, 292 (2007).

[40] N. Tsoneva and H. Lenske, Phys. Rev. C **77**, 024321 (2008).

[41] A. P. Tonchev, S. L. Hammond, J. H. Kelley, E. Kwan, H. Lenske, G. Rusev, W. Tornow, and N. Tsoneva, Phys. Rev. Lett. **104**, 072501 (2010).

[42] V. Derya, N. Tsoneva, T. Aumann, M. Bhike, J. Endres, M. Gooden, A. Hennig, J. Isaak, H. Lenske, B. Loher, N. Pietralla, D. Savran, W. Tornow, V. Werner, and A. Zilges, Phys. Rev. C **93**, 034311 (2016).
[43] H. Lenske and N. Tsoneva, Eur. Phys. J. A **55**, 238 (2019).
[44] N. V. Antonenko and L. A. Malov, Izv. RAN, Ser. Phys. **78**, 1402 (2014).
[45] G. G. Adamian, N. V. Antonenko, H. Lenske, and L. A. Malov, Phys. Rev. C **101**, 034301 (2020).
[46] G. G. Adamian, N. V. Antonenko, H. Lenske, S. V. Tolokonnikov, and E. E. Saperstein, Phys. Rev. C **94**, 054309 (2016).
[47] I. S. Rogov, G. G. Adamian, N. V. Antonenko, and T. M. Shneidman, Nucl. Phys. A **1002**, 121995 (2020).
[48] N. Wang, M. Liu, X. Wu, and J. Meng, Phys. Lett. B **734**, 215 (2014); http://www.imqmd.com/mass/
[49] J. Dudek, Z. Szymanski, T. Werner, A. Fäßler, and C. Lima, Phys. Rev. C **26**, 1712 (1982).
[50] N. Schwierz, I. Wiedenhöver, and A. Volya, arXiv:0709.3525.
[51] A. Rahmatinejad, A. N. Bezbakh, T. M. Shneidman, G. Adamian, N. V. Antonenko, P. Jachimowicz, and M. Kowal, Phys. Rev. C **103**, 034309 (2021).
[52] http://www.nndc.bnl.gov/ensdf
[53] G. Audi, F. G. Kondev, M. Wang, W. J. Huang, and S. Naimi, Chin. Phys. C **41**, 030001 (2017).
[54] R. Smolańczuk, Phys. Rev. C **56**, 812 (1997).
[55] V. M. Strutinsky, Ark. Fys. **36**, 629 (1966).
[56] J. L. Egido and A. Jungclaus, Phys. Rev. Lett. **125**, 192504 (2020).
[57] P.-G. Reinhard, Rep. Prog. Phys. **52**, 439 (1989).
[58] G. Colò, N. Van Giai, and H. Sagawa, Phys. Lett. B **363**, 5 (1995).
[59] J. Bartel, P. Quentin, M. Brack, C. Guet, and H. B. Håkansson, Nucl. Rev. A **386**, 79 (1982).
[60] E. Chabanat, P. Bonche, P. Haensel, J. Meyer, and F. Schaeffer, Nucl. Rev. A **635**, 231 (1998).
[61] T. Lesinski, M. Bender, K. Bennaceur, T. Duguet, and J. Meyer, Phys. Rev. C **76**, 014312 (2007).